Article

Effect of Doped Hole Transporting Layer on the Perovskite Solar Cell Performances

Min Ji Kwon , Hyesu Lee , Ji Yoon Jung , Jae-Woong Yu *

Posted Date: 11 December 2023

doi: 10.20944/preprints202312.0677.v1

Keywords: Perovskite solar cells; Doped hole transporting layer; Microwave annealing; Post-annealing; Long-term stability

Article

Effect of Doped Hole Transporting Layer on the Perovskite Solar Cell Performances

Min Ji Kwon, Hyesu Lee and Ji Yoon Jung Jae-Woong Yu *

Department of Advanced Materials Engineering for Information & Electronics, Kyung Hee University, 1732 Deogyeong-daro, Giheung-gu, Yongin, Gyeonggi, 17104, Korea

* Correspondence: authors: *jwyu@khu.ac.kr (J.-W. Yu)*

Abstract: The influences of doped hole transporting layer (HTL) on the performances of perovskite solar cells were studied. The influences of electrostatic and surface roughness effect by solvent additive doping were compared. The electrostatic effect of solvent additive doping was compared by addition of 1,8-diiodooctane and 1,8-dichlorooctane to the HTL layer. The surface roughness effect of solvent additive doping was examined using atomic force microscopy. The perovskite crystallinity by doping HTL was studied by X-ray diffraction. The conductivity of HTL was measured using four probe methods and was higher for doped devices. Enhanced conductivity of PEDOT:PSS film was also proved using fluorescence emission quenching. Long-term stability of the device was enhanced by doping HTL. The device with solvent additive exhibited much enhanced stability, retained over 80% of the initial PCE for 400 hours, while PCE of the device without solvent additive decreased to less than 80% after 200 hours. A very weak power microwave treatment was used for post-annealing of the fully fabricated devices. Post-annealing enhanced the lifetime of the device. Comparing different size of cells, the device lifetime was decreased as the cell area increased and as the size of the cell increased, the extent of lifetime enhancement by doping was increased.

Keywords: perovskite solar cells; doped hole transporting layer; microwave annealing; post-annealing; long-term stability

1. Introduction

Several emerging solar cells (i.e. Organic, Dye-sensitized, Quantum dot and Perovskite) have received growing attentions because of the necessity for sustainable and clean energy. Among these emerging solar cells, perovskite solar cells (PSCs) show the sharpest increase in efficiency. PSCs started with an efficiency of 3.8 % in 2009 [1] and achieved an efficiency of 26.1% in 2023 [2]. Now days the efficiency of the PSCs has developed to the point where it matches to that of the crystalline silicon solar cells. However, the PSCs are vulnerable to heat and moisture, making them difficult to commercialize due to its low stability and short lifetime. Silicon solar cells are known to have a lifetime of more than 30 years, but typical perovskite cells have a lifetime of less than a year. Therefore, it is necessary to improve stability of perovskite solar cells for the commercialization.

Another problem for the commercialization of PSCs is that it is difficult to prepare a uniform large-area perovskite film through a single solution process, because the uniformity of the formed film varies greatly depending on various conditions. The key points for fabrication of the efficient PSCs are how to make the minimal defect films without pinhole and with a large grain. The inverted structure (i.e. n-i-p type) is widely used because of mass production capability using low temperature solution processing and negligible hysteresis behavior [3–5]. Poly(3,4-ethylenedioxythiophene) : poly(styrenesulfonate) (PEDOT:PSS) has widely used in the inverted PSCs because of its low temperature processability, good electrical conductivity and mass production capability such as roll-to-roll processing. The conductivity of PEDOT:PSS films from stock solution is usually below 1 S/cm, which is much lower than those of metal or inorganic cathode materials. Therefore, the conductivity of PEDOT:PSS films should be increased.

The uniformity of PEDOT:PSS film morphology is also important to the PSCs' performance. Recently many studies [6–15] have been reported for the doping of the PEDOT:PSS film which

 doi:10.20944/preprints202312.0677.v1

improve the uniformity and roughness of the hole transporting layers. The addition of dopants increases the uniformity of the PEDOT:PSS film and consequently improves the efficiency and stability of the PSCs devices. In this study, we studied for a novel processing technology to improve performances of PSCs by adding solvent additives to PEDOT:PSS. 1,8-diiodooctane (DIO) and 1,8-dichlorooctane (DCO), high boiling liquids which miscible in methanol, are widely used as a surfactant for controlling phase separation of active materials in organic solar cell industry. DIO is seldom used with PEDOT:PSS and a reduction of PEDOT:PSS film when mixed with DIO was reported [16]. It is expected that addition of these solvent additives would produce a more homogeneous PEDOT:PSS films with higher conductivity and the partially electro negative halogen (i.e. $I^{\delta-}$ and $Cl^{\delta-}$) in the DIO and DCO could interact with Pb^{2+} of the perovskite crystal while the hydrophobic aliphatic moiety (i.e. partially positive octyl groups) can passivate surface of perovskite thin film from moisture.

2. Materials and Methods

2.1. Device fabrication

The 2.5cm x 2.5cm ITO (17 Ω per square) glass was ultrasonically washed with acetone, isopropyl alcohol, and acetone for 10 minutes each, sequentially. After drying ITO glass, it was surface treated with UV-O_3 for 40 minutes, then the prepared PEDOT:PSS (Clevios AI 4083) solution was spin-coated at 4500 rpm for 50s. For doping process, a 1,8-diiodooctane (DIO, purchased from Sigma-Aldrich) or 1,8-dichlorooctane (DCO, purchased from Sigma-Aldrich) was added to the PEDOT:PSS solution. The doped PEDOT:PSS solutions were dispersed using ultrasonication for at least 1 hour and doping ratio was 1 wt%, 1.5 wt%, 2 wt%, and 2.5 wt%, respectively. The remaining solvent was dried by thermal treatment in an oven at 120 °C or by microwave treatment at 200 W for two 10 s (10 seconds rest between treatment). A perovskite precursor solution was prepared by mixing lead iodide (PbI_2, 99.99 %, purchased from TCI) 290 mg, methyl ammonium iodide (MAI, 99 %, purchased from Sigma-Aldrich) 111.3 mg, lead (II) chloride ($PbCl_2$, 99.999 %, purchased from Alfa Aesar) 19.5 mg in a solvent mixture of N,N-dimethyl formamide (DMF, 99.8 %, purchased from Sigma-Aldrich) 0.45ml and dimethyl sulfoxide (DMSO, 99.9 %, purchased from Sigma-Aldrich) 0.05ml. The mole ratio of PbI_2 : $PbCl_2$ was 9 : 1 and [PbI_2 + $PbCl_2$] : MAI was 1 : 1. This perovskite precursor solution was spin coated on top of the hole transport layer, at 1000 rpm for 10 s and then at 4000 rpm for 20 s, and then 0.4 ml of diethyl ether (99.7 %, purchased from Sigma-Aldrich), which is an anti-solvent, was sprayed and annealed at 100 °C for 10 minutes. Phenyl-C_{60}-butyric acid methyl ester ($PC_{60}BM$, 98.5 %, purchased from Nano-C) solution, prepared by dissolving 7.5 mg of $PC_{60}BM$ in 0.5 ml chlorobenzene (CB, 99.8 %, purchased from Sigma-Aldrich) at 40 °C, was spin coated to the formed perovskite film at 2000 rpm for 40 s and dry at 80 °C oven for 5 minutes. 0.5 mg bathocuproine (BCP, purchased from Luminescence Technology Corp.) dissolved in 1 ml of ethanol was spin coated at 2000 rpm for 30 s to form a buffer layer. Finally, a 100 nm thick silver electrode was deposited through a thermal evaporator on top of the BCP layer. The active area of each device was 9.00 mm^2. For post-annealing microwave treatment, a low-powered microwave (at 50 W) was irradiated for 5 s.

2.2. Characterization

J-V characteristics were measured using a Keithley 2400 Source Measure Unit and McScience K201 LAB55 solar simulator under AM 1.5 (100 mW/cm) condition. Measurements were not corrected for reflection loss or light absorption in the ITO electrode. The surface morphologies, average and root mean square roughness of the perovskite film were evaluated using an atomic force microscope (AFM : S.I.S. GmbH, Germany). The information on surface topography and composition of the perovskite films was analyzed using a scanning electron microscope (SEM : Hitach, TM3000). The perovskite crystalline structure was analyzed by an X-ray diffractometer (XRD : Rigaku MiniFlex 300).

Preprints (www.preprints.org) | NOT PEER-REVIEWED | Posted: 11 December 2023 doi:10.20944/preprints202312.0677.v1

3. Results and Discussion

The main target of this study is to enhance the performances of PSCs to be more realistic for commercialization of PSCs. A solvent additive doped PEDOT:PSS was used as a hole transporting layer of invert type PSCs which known as a favorable processing method to prepare a large-scale PSCs because of the formation of a smooth surface and a more uniform perovskite layer through the electrostatic effect of the solvent additives contained in the PEDOT:PSS [17]. It is well known that the quality of perovskite grain growth is affected by the smoothness of the PEDOT:PSS layer [18–20]. DIO has widely used as a surfactant in organic solar cell industry to improve the morphology and control phase separation of two immiscible donor-acceptor materials. DIO also used as an additive for perovskite precursor solution to improve the crystallinity of the perovskite crystal [21,22].

The optimum solvent additive doping rate was obtained by changing composition ratio of dopant DIO against PEDOT:PSS. Figure 1 shows the change in the open circuit voltage (Voc), short circuit current density (Jsc), fill factor (FF), power conversion efficiency (PCE) according to the composition ratio of the additive.

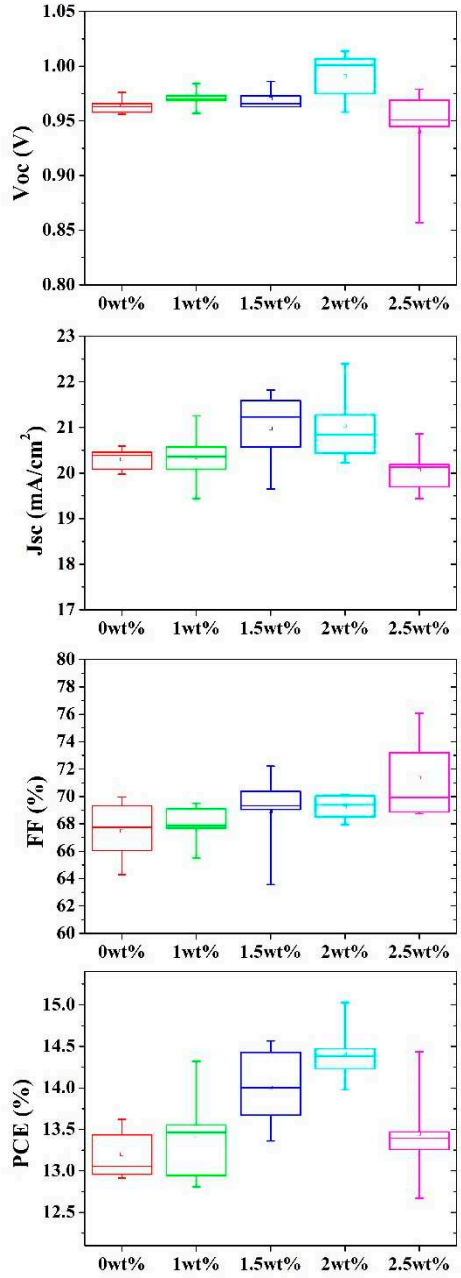

Figure 1. Device parameters as a function of solvent additive (DIO) composition.

Preprints (www.preprints.org) | NOT PEER-REVIEWED | Posted: 11 December 2023 doi:10.20944/preprints202312.0677.v1

The device performances are summarized in Table 1.

Table 1. Averaged device performances according to DIO doping concentrations.

C (wt%)	Voc (V)	Jsc (mA/cm²)	FF (%)	PCE (%)
0	0.964±0.008	20.30±0.26	67.47±2.34	13.20±0.31
1	0.971±0.010	20.35±0.67	67.93±1.57	13.42±0.60
1.5	0.970±0.010	20.97±0.88	68.91±3.23	14.01±0.50
2.5	0.940±0.048	20.07±0.54	71.37±3.19	13.44±0.64

All of the measured device performances were averaged over at least 10 devices. The best device performance was obtained with 2 wt% doping ratio and the Voc, Jsc, FF, and PCE of PSC at AM 1.5 100 mW/cm² condition were 0.991 ± 0.024 V, 21.04 ± 0.86 mA/cm², 0.692 ± 0.010, and 14.42 ± 0.39 %, respectively. Since the best device performance was obtained with 2 wt% doping condition, all other studies were proceeded with this doping ratio. The PCE of the device fabricated on the un-doped PEDOT:PSS layer with conventional thermal annealing was 13.20 ± 0.31. Therefore, it can be concluded that doped PEDOT:PSS hole transporting layer increased the PCE of the device about 10%.

To find out electrostatic effect of dopant (i.e. the surface ion density of the hole transporting layer) on the device performances, the solvent additive DIO was changed to 1,8-dichlorooctane (DCO). Since electronegativity of chlorine atom (3.16) is higher than that for iodine atom (2.66), Pb^{2+} ions included in perovskite crystal should be more strongly held through electrostatic interaction between chlorine atoms and lead ions. The devices were prepared as same method as DIO; however, due to the molecular weight differences between iodide and chlorine (the molecular weight of DCO is 183.12 g/mol, while that for DIO is 366.02g/mol), the same dopant mole ratio to PEDOT was reduced to 1 wt%. Table 2 summarizes the device performances with DCO as a dopant. Once again, the device doped with 1 wt% DCO showed the best device performances.

Table 2. Averaged device performances according to DCO doping concentrations.

C (wt%)	Voc (V)	Jsc (mA/cm²)	FF (%)	PCE (%)
0	1.023±0.005	19.37±0.59	66.85±0.88	13.24±0.23
0.5	1.031±0.003	20.77±0.71	64.34±3.52	13.76±0.31
0.75	1.031±0.008	21.00±0.89	65.57±3.81	14.17±0.52
1	1.027±0.008	20.68±0.62	67.29±3.78	14.27±0.52
1.25	1.026±0.025	19.91±1.41	68.96±4.22	14.06±0.48

The Voc, Jsc, FF, and PCE of PSC at AM 1.5 100 mW/cm² condition were 1.027 ± 0.008 V, 20.68 ± 0.62 mA/cm², 0.673 ± 0.038, and 14.27 ± 0.52 %, respectively. The PCEs of the devices doped with DIO and DCO were within the experimental error range, so that it could conclude that the electrostatic effect of dopant on the device performance was very weak.

The surface roughness effect on the device performances was tested by preparing three different hole transporting layers (un-doped PEDOT:PSS film, DIO-doped PEDOT:PSS film, DCO-doped PEDOT:PSS film). Perovskite film was fabricated on these hole transporting layers by one-step method explained in "Experimental" section. Figure 2 shows AFM topology images of the perovskite grain fabricated on these hole transporting layers.

Preprints (www.preprints.org) | NOT PEER-REVIEWED | Posted: 11 December 2023 doi:10.20944/preprints202312.0677.v1

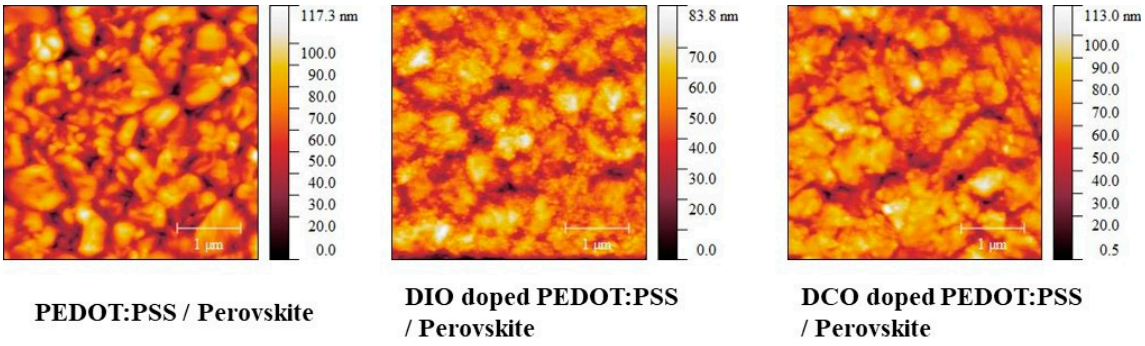

Figure 2. AFM topology images of the perovskite grain fabricated on three different hole transporting layers.

The rms (root mean square) roughness values were 17.15 nm, 10.83 nm and 13.59 nm, respectively. The surface roughness was the lowest for the perovskite film coated on the DIO-doped PEDOT:PSS layer. Since the perovskite film was formed on PEDOT:PSS layer, it was concluded that the smoother the PEDOT:PSS film, the smoother the perovskite film. To study the effect of doping on perovskite crystallinity, X-ray diffraction (XRD) analysis was proceeded. Figure 3 shows the XRD images of the film formed on the three different hole transporting layers.

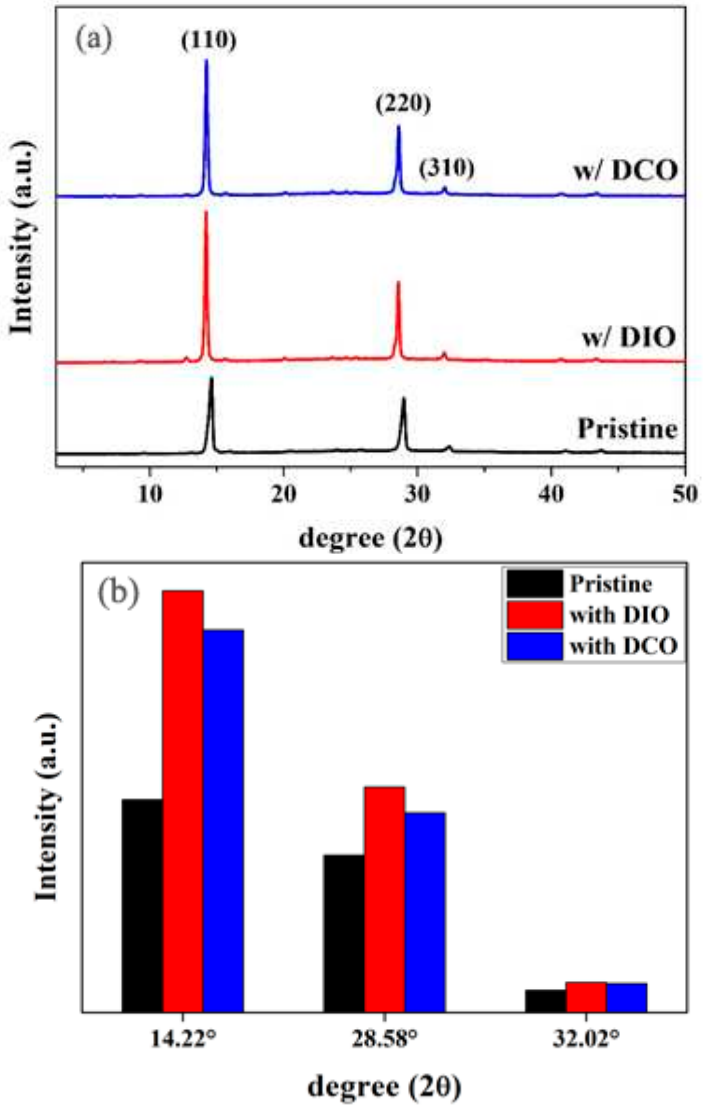

Preprints (www.preprints.org) | NOT PEER-REVIEWED | Posted: 11 December 2023 doi:10.20944/preprints202312.0677.v1

Figure 3. (a) XRD images for the three different hole transporting layers, (b) the plane diffraction peak intensity ratio of each layer.

Diffraction peaks appeared at 2θ = 14, 28, and 32°, which assign to the (110), (220), and (310) planes of the tetragonal $CH_3NH_3PbI_3$ perovskite structures [23]. Comparing the XRD peak intensity, it was clear that the crystallinity of perovskite films formed on the doped hole transporting films (both DIO and DCO) were higher. The surface roughness effect on the device performances was studied by forming device on these three different hole transporting layers. The external quantum efficiency (EQE) measurement as shown in Figure 4 confirms the higher photon absorption in the range of 350 - 800 nm for the PSCs with additives compared to that for without additives.

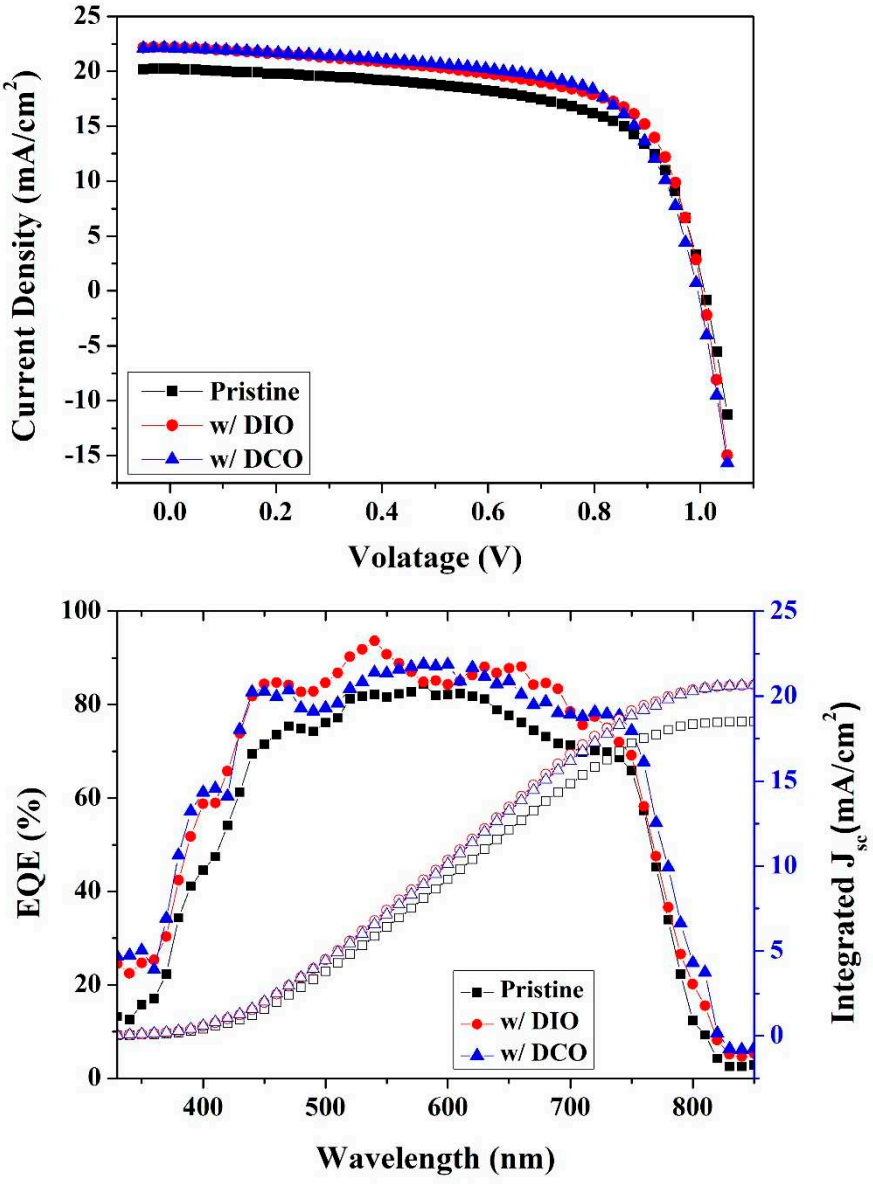

Figure 4. J-V curve and external quantum efficiency of the devices.

The integral current density of the EQE spectra over the AM 1.5G solar emission spectrum shows over 20 mA/cm² for the device with additives and about 18 mA/cm² for the device without additives. The trend of EQE spectra was consistent with the results of the I-V curve. The PCE of the device formed on the doped hole transporting films (both DIO and DCO) showed about 10% enhanced efficiency compare to that for formed on un-doped hole transporting film (Tables 1 and 2). This increase is exactly the same amount as the increase in PCE by doping the PEDOT:PSS layer.

Preprints (www.preprints.org) | NOT PEER-REVIEWED | Posted: 11 December 2023 doi:10.20944/preprints202312.0677.v1

To analyze the doping effect on the conductivity of PEDOT:PSS layer, the sheet resistance was measured using four probe methods [24]. The sheet resistances of un-doped PEDOT:PSS film, DIO-doped PEDOT:PSS film, DCO-doped PEDOT:PSS film coated on ITO glass were 181.8, 161.4 and 163.6 Ω, respectively. The thickness of the film that required to obtain this sheet resistance was measured by SEM, which turned out to be 30.6 nm. The final conductivity of un-doped PEDOT:PSS film, DIO-doped PEDOT:PSS film, DCO doped PEDOT:PSS film were 1796, 2023, 1996 S/cm, respectively. The solvent additive doping of PEDOT:PSS increased the conductivity of PEDOT:PSS film. The conductivity of both DIO- and DCO-doped PEDOT:PSS film were within the experimental error range, so that it could conclude that the conductivity of these doped PEDOT:PSS film were same. Combining these electrostatic, surface roughness and conductivity results, the device performance enhancement was mainly caused by smoother surface formation and conductivity increase by doping HTL.

Enhancement in the conductivity of PEDOT:PSS film was also proved by increase in the charge transfer rate of the perovskite crystal to PRDOT:PSS. To evaluate the charge transfer from the perovskite layer to PEDOT:PSS film, fluorescence emission intensity was measured using a structure of ITO/PEDOT:PSS (with or without solvent additive)/perovskite sample. As shown in Figure 5, a greater extent of fluorescence emission quenching (i.e. emission intensity decrease) was observed in the sample with DIO (device with microwave annealing showed higher emission quenching), indicating that the sample with DIO additive exhibited slightly higher quenching efficiency of excited state and better hole transport ability than the device with bare PEDOT:PSS.

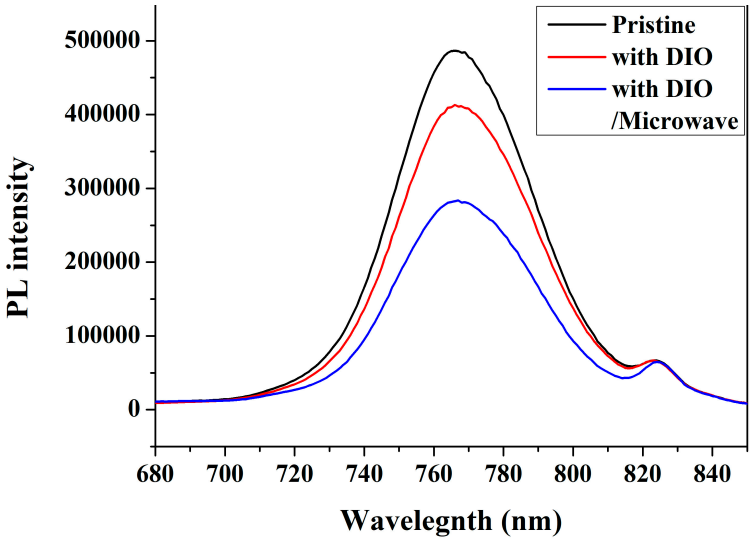

Figure 5. Fluorescence emission spectra of the perovskite films deposited on bare PEDOT:PSS and DIO-doped PEDOT:PSS.

Stability of the devices was tested using un-doped, DIO-doped and DCO-doped PEDOT:PSS films by measuring the time required for the PCE to fall below 80% of the initial value (LT80). The PCE measurements were proceeded at room temperature under ambient air conditions without device encapsulation. Figure 6 shows the PCE changes with time for these devices.

Preprints (www.preprints.org) | NOT PEER-REVIEWED | Posted: 11 December 2023 doi:10.20944/preprints202312.0677.v1

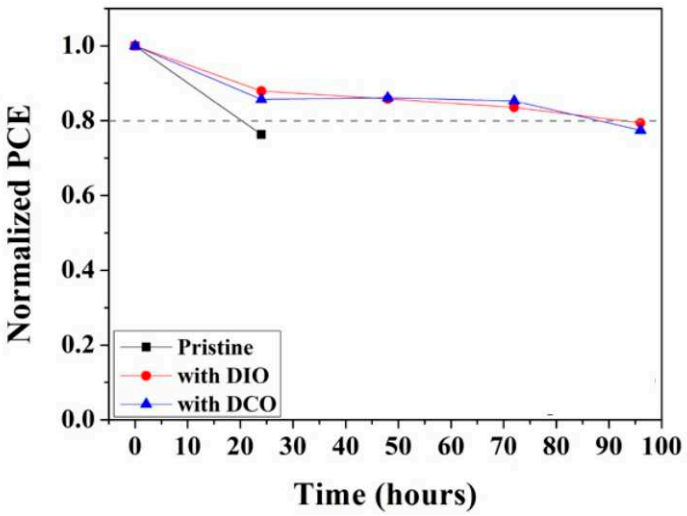

Figure 6. PCE changes of the devices with undoped, DIO-doped and DCO-doped PEDOT:PSS films as a function of time at 35% relative humidity condition without encapsulation.

The device with un-doped PEDOT:PSS film showed LT80 of 20 hours, while those of devices with both DIO- and DCO-doped PEDOT:PSS film showed LT80 of about 90 hours, which increased by 4.5 times compared to pristine device with un-doped PEDOT:PSS film. This enhancement in device stability was resulted from the passivation effect of the bottom of the perovskite by the additive alkyl di-halides [14]. DIO showed slightly better LT80 between doping with DIO and DCO, and the XRD intensity and AFM roughness values were also slightly better for DIO-doped devices so that all devices were prepared with DIO doping.

PEDOT:PSS nanoparticles are dispersed in distilled water, it takes long time to anneal this spin coated PEDOT:PSS hole transporting layer (usually takes more than 10mins), which is another obstacle to the use of mass production methods such as roll-to-roll processing. Microwave annealing process was proceeded with a home-made power adjustable microwave equipment and compared with the conventional thermal annealing. The power of microwave was set to 200 W (power of general microwave oven is usually 800 ~ 1,000 W) and the PEDOT:PSS film was annealed for 10 s, rest for 10 s and annealed for another 10 s. The overall time required for microwave annealing was only 30 s, which is par less than that required for the conventional thermal annealing (typically 15 mins in 120 °C oven). Table 3 summarizes the device performances according to annealing conditions.

Table 3. Device performances according to annealing method.

Conditions	Voc (V)	Jsc (mA/cm²)	FF (%)	PCE (%)
Thermal, undoped	0.964±0.008	20.30±0.26	67.47±2.34	13.20±0.31
Thermal, 2wt% DIO	0.991±0.024	21.04±0.86	69.20±0.97	14.42±0.39
Microwave, 2wt% DIO	0.988±0.019	20.64±1.09	70.91±2.83	14.44±0.54

The PCE of the device fabricated on the un-doped PEDOT:PSS film with conventional thermal annealing was 13.20 ± 0.31. While that for devices on 2 wt% DIO-doped PEDOT:PSS film was 14.42 ± 0.39 % for thermal annealing and 14.44 ± 0.54 for microwave annealing. Doping HTL increased the PCE of the device about 10%. When comparing annealing condition between microwave and thermal annealing, all device parameters (i.e. Voc, Jsc, FF, and PCE) were quite similar; therefore, it could be concluded that microwave annealing could provide the same device performance, while reducing processing time by 1/30th compared to thermal annealing.

The effect of post-annealing was studied using a very weak power microwave. The conventional microwave power is too strong that it cannot be used for fully fabricated devices (i.e. the device with metal electrode) because of reflection from the surface of metal. In this post-annealing study, the power of microwave was set to 50 W to penetrate through the metal electrode and vaporized the trace

Preprints (www.preprints.org) | NOT PEER-REVIEWED | Posted: 11 December 2023 doi:10.20944/preprints202312.0677.v1

of moisture that contained inside of the device during fabrication processes. The fully fabricated devices were exposed to microwave for only 5 secs. The PCE was measured before and after microwave treatment. The fabricated devices were stored at ambient condition with relative humidity of 35% without device encapsulation. Table 4 summarizes the PCE changes as a function of time.

Table 4. The PCE change for post-annealing treatment.

		As prepared (%)	1 day (%)	2 days (%)	3 days (%)	4 days (%)	5 days (%)
Undoped	Before Microwave	12.69	9.01	-	-	-	-
	After Microwave	13.20	10.07	-	-	-	-
DIO doped	Before Microwave	14.44	12.10	11.88	11.57	11.37	10.71
	After Microwave	14.61	12.84	12.54	12.21	11.60	11.19

Both un-doped and doped devices showed enhanced PCE after microwave treatment. The un-doped device failed one day after fabrication, while the DIO-doped device survived for 5 days and showed enhanced PCE after microwave treatment. From these results, it can be concluded that a low power microwave treatment could vaporize the trace of moisture and prolong the lifetime of the device.

To more effectively check the effect of doping on increasing the stability and lifetime of the devices, the active area was doubled in width and length. The area of cell was increased from 0.09 cm^2 to 0.36 cm^2. Table 5 summarizes the best PCE of small and large-area device with different conditions.

Table 5. Small and large-area device best performances with different annealing method.

Conditions	V_{OC} (V)	J_{SC} (mA/cm^2)	FF (%)	PCE (%)
Undoped (0.09cm^2)	0.963	20.40	69.32	13.62
2wt% DIO (0.09cm^2)	0.958	22.40	70.04	15.03
2wt% + Microwave (0.09cm^2)	0.990	21.35	70.77	14.96
Undoped (0.36cm^2)	0.849	19.19	61.15	9.96
2wt% DIO (0.36cm^2)	0.872	21.11	65.97	12.15
2wt% + Microwave (0.36cm^2)	0.869	21.25	66.14	12.21

The PCE of thermally annealed un-doped cell for 0.09 cm^2 was 13.62 %, while that for 0.36 cm^2 was 9.96 %. The PCE of thermally annealed 2 wt% DIO-doped cell for 0.09 cm^2 was 15.03 %, while that for 0.36 cm^2 was 12.15 %. The PCE of larger area cell was reduced less (about 27 % reduction for un-doped cell and about 19 % reduction for un-doped cell) for DIO doped cell, probably due to the better areal uniformity caused by smoother hole transporting layer through doping the PEDOT:PSS layer. The PCE of microwave annealed 2 wt% DIO-doped cell for 0.09 cm^2 was 14.96 %, while that for 0.36 cm^2 was 12.21 %. The PCE drop of larger area cell was about 18 % for this microwave annealing condition. Once again, the microwave annealing didn't affect the device performance even for larger area cell. It could only reduce the time require for annealing to 1 / 30th compared to that of thermal annealing.

Long-term stability of the larger area device was also studied. The time required for LT80 condition was measured while the devices were exposure to 100 mW/cm^2 solar simulator light at relative humidity of 35% without device encapsulation [Figure 7(a) and (b)]. Figure 7(a) shows 0.09 cm^2 cell data, which LT80 for un-doped cell was 3.4 hours and that for 2 wt% DIO-doped cell was 5.3 hours. The lifetime of doped device was enhanced about 1.6 times compare that for un-doped device. Figure 7(b) shows 0.36 cm^2 cell data, which LT80 for un-doped cell was 2.7 hours and that for 2 wt% DIO-doped cell was 4.9 hours. The lifetime of doped larger size device was enhanced about 1.8 times compare to that for un-doped device. Even though the absolute value of LT80 for larger size cell

Preprints (www.preprints.org) | NOT PEER-REVIEWED | Posted: 11 December 2023 doi:10.20944/preprints202312.0677.v1

decreased as the cell area increased (i.e. in the case of doped cell: 5.3 hours for 0.09 cm^2 cell and 4.9 hours for 0.36 cm^2 cell); however, as the size of the cell increased, the extent of lifetime enhancement by doping increased (i.e. 1.6 times for 0.09 cm^2 cell and 1.8 times for 0.36 cm^2 cell). Since the device lifetime was very short when the device was exposed to solar simulator light without an encapsulation, and to mimic a more realistic situation, the device storage method was changed. The devices were stored at relative humidity of 35% without device encapsulation; however, Figure 7(c) and (d) show the PCE changes as a function of time for the devices stored in scattered light [Figure 7(c)] and in dark [Figure 7(d)]. Figure 7(c) shows the PCE changes for 0.09 cm^2 cell data, LT80s were dramatically increase compare to the devices exposed to the illumination with same device area [i.e. Figure 7(a)].

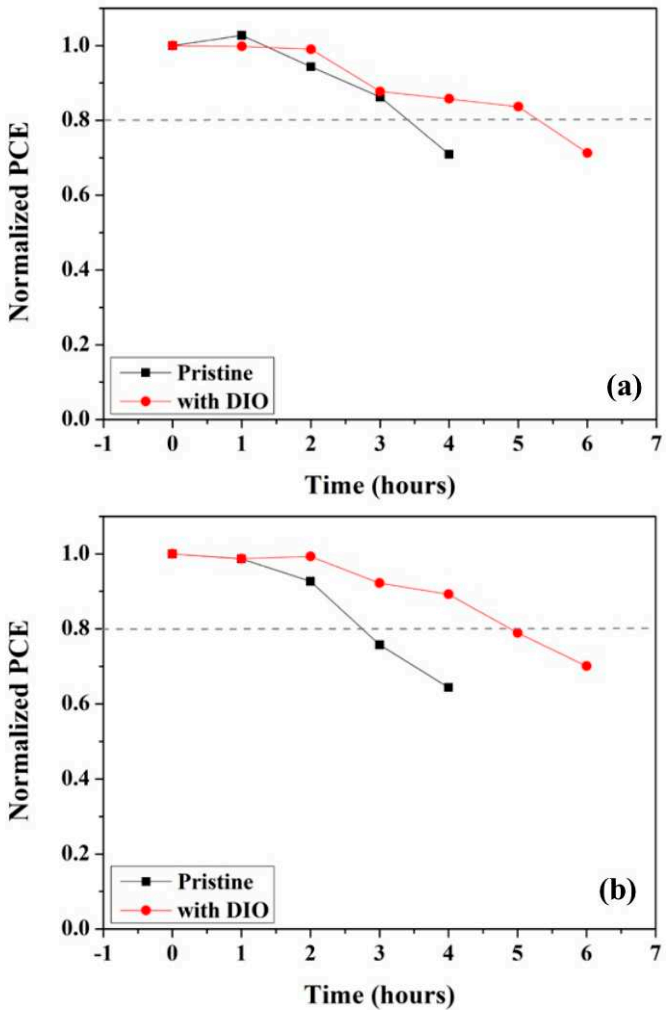

Preprints (www.preprints.org) | NOT PEER-REVIEWED | Posted: 11 December 2023 doi:10.20944/preprints202312.0677.v1

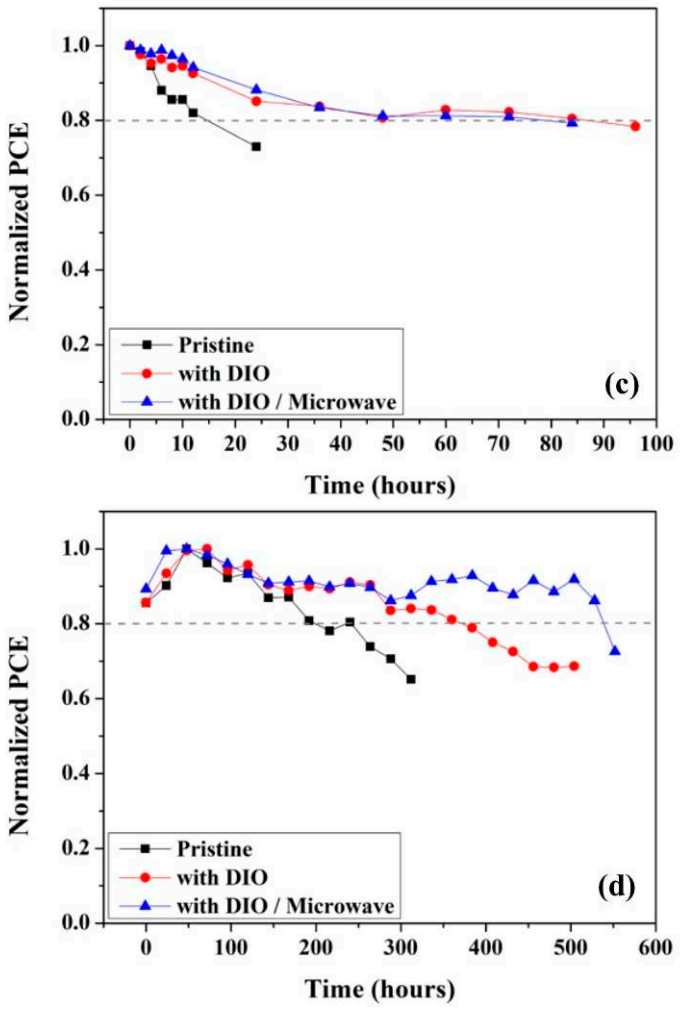

Figure 7. PCE changes as a function of time to obtain the LT80. (a) 0.09 cm² cell exposure to 100 mW/cm² solar simulator light at relative humidity of 35% without encapsulation, (b) 0.36 cm² cell exposure to 100 mW/cm² solar simulator light at relative humidity of 35% without encapsulation, (c) 0.09 cm² cell stored at relative humidity of 35% without device encapsulation, and (d) 0.36 cm² cell stored at relative humidity of 35% without device encapsulation.

LT80 for un-doped cell was 15 hours and that for 2 wt% DIO-doped cell was 78 hours. The lifetime enhancement for doped device was about 5.2 times compare that for un-doped device. Figure 7(d) shows the PCE changes for 0.36 cm² cell data, LT80 for un-doped cell was 192 hours and that for 2 wt% DIO-doped cell was 540 hours. The lifetime enhancement for doped device was about 2.8 times compare that for un-doped device. From these experiments, it could be concluded that the differences in the lifetime between un-doped and doped devices decreased when the devices were stored at the dark environment.

4. Conclusion

A novel processing technology to improve stability of PSCs by doping hole transporting layer was examined. The optimum doping rate was 2 wt% of DIO to PEDOT:PSS and this doping enhanced the PCE of the device about 10%. The electrostatic effect of dopant on the device performances was studied by changing the dopant DIO to DCO. Replacing the atoms in the dopant from diiodide to dichloride changed ion density of the HTL (because of differences in the electronegativity between chlorine and iodine) resulted in electrostatic interaction change between halide atoms of the dopant and lead ions of the perovskite crystal. Due to the molecular weight differences between iodide and chlorine, the same dopant mole ratio to PEDOT was reduced to 1 wt% and this composition showed the best device performances. The device performances were within the experimental error range, so

that it could conclude that the electrostatic effect was a very weak influence on the device performances.

The surface roughness effect on the device performances was examined using AFM. Doped HTL layer produced a smoother surface and resulting in smoother perovskite surface. According to XRD diffraction peak intensity study, the perovskite crystallinity formed on the doped HTL (both DIO and DCO) was higher. The conductivity of HTL was measured using four probe methods and was higher for doped devices. Combining these electrostatic, surface roughness and conductivity results, the enhancement of the device performance was mainly caused by smoother surface formation and increase in conductivity rather than the electrostatic interaction.

Long-term stability of the device was tested by measuring the time required for the PCE to fall below 80% of the initial value. DIO doping appeared to be slightly better DCO doping on the device performances. When 200 W microwave was used to anneal PEDOT:PSS film, the processing time was reduced to 1 / 30th of thermal annealing without losing device performances. A lower power (50 W) microwave treatment was used for post-annealing of the fully fabricated devices, and it turn out to vaporize the trace of moisture and prolong the lifetime of the device. The stability enhancement was studied using larger area cell, the doped devices showed much enhanced device lifetime compared to that for un-doped device. According to larger size cell studies, the device lifetime was decreased as the cell area increased; however, as the size of the cell increased, the extent of lifetime enhancement by doping increased. These enhancements of long-term stability were attributed to the passivation process. The partially electro negative halogen (i.e. $I^{\delta-}$ and $Cl^{\delta-}$) in the DIO and DCO could interact with Pb^{2+} of the perovskite crystal while the hydrophobic aliphatic moiety (i.e. partially positive octyl groups) can passivate surface of perovskite thin film from moisture. This passivation effect by surface modification of the perovskite grains could be beneficial for the long-term stability of devices and is well studied [14,25–28].

Acknowledgments: This work was supported by the National Research Foundation of Korea (NRF) grant funded by the Korea government (MSIT) (Grant No. 2022R1F1A1070498, All solution processed thin film encapsulation film for flexible electronics).

References

1. Kojim, A.; Teshima, K.; Shirai, Y.; Miyasaka, T. Organometal Halide Perovskites as Visible-Light Sensitizers for Photovoltaic Cells, *J. Am. Chem. Soc.* 2009,*131*, 6050 - 6051. https://doi.org/10.1021/ja809598r.
2. Best research-cell efficiency chart, NREL (2023). https://www.nrel.gov/pv/cell-efficiency.html.
3. Luo D.; Yang W.; Wang Z.; Sadhanala A.; Hu Q.; Su R.; Shivanna R.; Trindade G.F.; Watts J.F.; Xu Z.; Liu T.; Chen K.; Ye F.; Wu P.; Zhao L.; Wu J.; Tu Y.; Zhang Y.; Yang X.; Zhang W.; Friend R.H.; Gong Q.; Snaith J.H.; Zhu R. Enhanced photovoltage for inverted planar heterojunction perovskite solar cells, *Science* 2018, *360*, 1442 - 1446. https://doi.org/10.1126/science.aap9282.
4. Yip H.-L.; Jen A.K.-Y. Recent advances in solution-processed interfacial materials for efficient and stable polymer solar cells. *Energy Environ. Sci.* 2012, *5*, 5994 - 6611. https://doi.org/10.1039/C2EE02806A.
5. Liu T.; Chen K.; Hu Q.; Zhu R.; Gong Q. Inverted perovskite solar cells: progresses and perspectives, *Adv. Energy Mater.* 2016, *6*, 1600457. https://doi.org/10.1002 /aenm.201600457.
6. Hu Y.; Tang Y.; Zhang Z.; Yang F.; Jiang L.; Song Y.; Liu H. Improving the efficiency of inverted perovskite solar cells by Bis (acetylacetonato) dioxomolybdenum (VI)-doped PEDOT: PSS, *Mater. Lett.* 2022, *306*, 130911. https://doi.org/10.1016/ j.matlet.2021.130911.
7. Xu L.; Li Y.; Zhang C.; Liu Y.; Zheng C.; Lu W.; Li M.; Chen Y.; Huang W.; Chen R. Improving the efficiency and stability of inverted perovskite solar cells by CuSCN-doped PEDOT: PSS, *Solar Energy Mater. Solar Cells* 2020, *206*, 110316. https://doi.org/10.1016/j.solmat.2019.110316.
8. Liu D.; Li Y.; Yuan J.; Hong Q.; Shi G.; Yuan D.; Wei J.; Huang C.; Tang J.; Fung M.-K. Improved performance of inverted planar perovskite solar cells with F4-TCNQ doped PEDOT: PSS hole transport layers, *J. Mater. Chem.* 2017, *A5*, 5701-5708. https://doi.org/10.1039/C6TA10212C.
9. Niu J.; Yang D.; Ren X.; Yang Z.; Liu Y.; Zhu X.; Zhao W.; Liu S. Graphene-oxide doped PEDOT: PSS as a superior hole transport material for high-efficiency perovskite solar cell, *Org. Electron.* 2017, *48*, 165-171. https://doi.org /10.1016 /j.orgel.2017.05.044.
10. Redondo-Obispo C.; Ripollesa T.S.; Cortijo-Campos S.; Álvareza A.L.; Climent-Pascual E.; de Andrés A.; Coya C. Enhanced stability and efficiency in inverted perovskite solar cells through graphene doping of PEDOT: PSS hole transport layer, *Mater. Design* 2020, *191*, 108587. https://doi.org/10.1016/j.matdes.2020. 108587.

11. Hu L.; Sun K.; Wang M.; Chen W.; Yang B.; Fu J.; Xiong Z.; Li X.; Tang X.; Zang Z.; Zhang S.; Sun L.; Li M. Inverted planar perovskite solar cells with a high fill factor and negligible hysteresis by the dual effect of NaCl-doped PEDOT: PSS, *ACS Appl. Mater. Interfac.* 2017, 9, 43902-43909. https://doi.org/10.1021/acsami.7b14592.
12. Jiang K.; Wu F.; Zhang G.; Chow P.C.Y.; Ma C.; Li S.; Wong K.S.; Zhu L.; Yan H. Inverted planar perovskite solar cells based on CsI-doped PEDOT: PSS with efficiency beyond 20% and small energy loss, *J. Mater. Chem.* 2019, *A7*, 21662-21667. https://doi.org/10.1039/C9TA08995K.
13. Huang P.; Liu Y.; Zhang K.; Yuan L.; Li D.; Hou G.; Dong B.; Zhou Y.; Song B.; Li Y. Catechol derivatives as dopants in PEDOT: PSS to improve the performance of p–i–n perovskite solar cells, *J. Mater. Chem.* 2017, *A5*, 24275-24281. https://doi.org /10.1039/C7TA08827B.
14. Zhu Y.; Wang S.; Ma R.; Wang C. The improvement of inverted perovskite solar cells by the introduction of CTAB into PEDOT: PSS, *Solar Energy* 2019, *188*, 28-34. https://doi.org/10.1016/j.solener.2019.05.073.
15. Erazoa E.A.; Castillo-Bendeck D.; Ortiz P.; Cortés M.T. NaCl doped electrochemical PEDOT: PSS layers for inverted perovskite solar cells with enhanced stability, *Synth. Met.* 2019, *257*, 116178. https://doi.org/10.1016/j.synthmet.2019.116178.
16. Wang W.; Qin F.; Zhu X.; Liu Y.; Jiang X.; Sun L.; Xie C.; Zhou Y. Exploring the Chemical Interaction between Diiodooctane and PEDOT-PSS Electrode for Metal Electrode-Free Nonfullerene Organic Solar Cell, *ACS Appl. Mater. Interfaces* 2020, *12*, 3800 - 3805. https://doi.org/10.1021/acsami.9b17321.
17. Xia Y.; Dai S. Review on applications of PEDOTs and PEDOT: PSS in perovskite solar cells, *J. Mater. Sci.: Mater. Electro.* 2021, *32*, 12746 - 12757. https://doi.org/10.1007/s10854-020-03473-w.
18. Wang Q.; Chueh C.-C.; Eslamian M.; Jen A.K.-Y. Modulation of PEDOT:PSS pH for efficient inverted perovskite solar cells with reduced potential loss and enhanced stability, *ACS Appl. Mater. Interfaces* 2016, *8*, 32068–32076. https://doi.org/ 10.1021/acsami.6b11757.
19. Xue Q.; Liu M.; Li Z.; Yan L.; Hu Z.; Zhou J.; Li W.; Jiang X.-F.; Xu B.; Huang F.; Li Y.; Yip H.-L.; Cao Y. Efficient and stable perovskite solar cells via dual functionalization of dopamine semiquinone radical with improved trap passivation capabilities. *Adv. Funct. Mater.* 2018, *28*, 1707444. https://doi.org/10.1002/adfm. 201707444.
20. Yang L.; Cai F.; Yan Y.; Li J.; Liu D.; Pearson A.J.; Wang T. Conjugated small molecule for efficient hole transport in high-performance p-i-n type perovskite solar cells. *Adv. Funct. Mater.* 2017, *27*, 1702613. https://doi.org/10.1002/adfm.201702613.
21. Kim J.H.; Williams S.T.; Cho N.; Chueh C.-C.; Jen A.K.-Y. Enhanced Environmental Stability of Planar Heterojunction Perovskite Solar Cells Based on Blade-Coating. *Adv. Energy Mater.* 2015, *5*, 1401229. https://doi.org/10.1002/aenm.201401229.
22. Liang P.-W.; Liao C.-Y.; Chueh C.-C.; Zuo F.; Williams S.T.; Xin X.-K.; Lin J.; Jen A.K.-Y. Additive enhanced crystallization of solution-processed perovskite for highly efficient planar-heterojunction solar cells, *Adv. Mater.* 2014, *26*, 3748-3754. https:// doi.org/10.1002/adma.201400231.
23. Zhao Y.; Zhu K. Optical Bleaching of Perovskite (CH_3NH_3)PbI_3 Through Room-Temperature Phase Transformation Induced by Ammonia, *Chem. Commun.* 2014, *50*, 1605-1607. https://doi.org/10.1039/C3CC48522F.
24. Miccoli I.; Edler F.; Pfnür H.; Tegenkamp C. The 100th anniversary of the four-point probe technique: the role of probe geometries in isotropic and anisotropic systems, *J. Phys. Condens. Matter* 2015, *27*, 223201. https://doi.org/10.1088/0953-8984/27/22/ 223201.
25. Zuo L.; Guo H.; deQuilettes D.W.; Jariwala S.; De Marco N.; Dong S.; DeBlock R.; Ginger D.S.; Dunn B.; Wang M.; Yang Y. Polymer-modified halide perovskite films for efficient and stable planar heterojunction solar cells, *Sci. Adv.* 2017, *3*, e1700106. https://doi.org/10.1126/sciadv.1700106.
26. Terry M.L.; Straub A.; Inns D.; Song D.; Aberle A.G. Large open-circuit voltage improvement by rapid thermal annealing of evaporated solid-phase-crystallized thin-film silicon solar cells on glass. *Appl. Phys. Lett.* 2005, *86*, 172108. https://doi.org /10.1063/1.1921352.
27. Li X.; Dar M.I.; Yi C.; Luo J.; Tschumi M.; Zakeeruddin S.M.; Nazeeruddin M.K.; Han H.; Grätzel M., Improved performance and stability of perovskite solar cells by crystal crosslinking with alkylphosphonic acid ω-ammonium chlorides, *Nature Chem.* 2015, *7*, 703 - 711. https://doi.org/10.1038/NCHEM.2324.
28. Wang Y.; Zhang T.; Kan M.; Zhao Y. Bifunctional Stabilization of All-Inorganic α-$CsPbI_3$ Perovskite for 17% Efficiency Photovoltaics, *J. Am. Chem. Soc.* 2018, *140*, 12345 - 12348. https://doi.org/10.1021/jacs.8b07927.